Article:
Galante, M., Ellis, M.O.A. orcid.org/0000-0003-0338-8920 and Sanvito, S. (2019) Nontrivial spatial dependence of the spin torques in L10 FePt-based tunneling junctions. Physical Review B, 99 (1). 014401. ISSN 2469-9950

https://doi.org/10.1103/physrevb.99.014401

Nontrivial spatial dependence of the spin torques in $L1_0$ FePt-based tunneling junctions

Mario Galante, Matthew O. A. Ellis, and Stefano Sanvito*
School of Physics and CRANN Institute, Trinity College Dublin, College Green, Dublin 2, Ireland

(Received 10 October 2018; revised manuscript received 21 November 2018; published 2 January 2019)

We present an *ab initio* study of the spin-transfer torque in Fe/MgO/FePt/Fe magnetic tunnel junctions. We consider an FePt film with a thickness up to six unit cells, either in direct contact with the MgO spacer or with an intercalated ultrathin Fe seed layer. We find that in the FePt layer the torque is not attenuated as strongly as in the case of pure Fe. Moreover, in FePt the torque alternates sign at the Fe and Pt atomic planes throughout the stack for all FePt thicknesses considered. Finally, when Fe is intercalated between MgO and $L1_0$ FePt, the torque is sharply attenuated, and it is transferred to FePt only for an Fe seed layer that is less than two atomic planes thick. We attribute these features to the different spatial profiles of the exchange and correlation field and the induced nonequilibrium spin accumulation. The calculated tunneling magnetoresistance of the Fe/MgO/FePt/Fe junctions studied is enhanced with respect to the one of Fe/MgO/Fe, while it is reduced with Fe intercalation. Our work shows that $L1_0$ FePt junctions can be promising candidates for current-operated magnetic devices and that the magnetic texture at the atomic scale has an important effect on the spin-transfer torque.

DOI: 10.1103/PhysRevB.99.014401

I. INTRODUCTION

Magnetic random access memories are believed to be among the most promising candidates to deliver the future of scalable, nonvolatile, rapidly accessible data storage [1]. At the heart of these devices are magnetic tunnel junctions (MTJs), which store data on the relative orientation of the magnetization vectors of two magnetic layers separated by an insulating barrier [2]. Reading and writing such junctions can be efficiently performed by applying an electric current through the device, exploiting the tunneling magnetoresistance (TMR) [3] effect for reading and using spin-transfer torque (STT) [4] to write. STT arises when a current passes across two ferromagnets having different magnetization directions, and it is caused by the transfer of angular momentum between the two mediated by the current. The conduction electrons become spin polarized by passing through the first magnetic layer, and their angular momentum is then transferred to the second. The ideal insulating barrier acts as a spin filter maximizing the spin polarization of the current and hence the torque.

Optimizing the device structure to achieve low write currents is an important challenge in realizing the potential of these devices. A stability analysis based on the Landau-Lifshitz-Gilbert equations of motion including the Slonczewski form of the spin-transfer torque (see Refs. [5,6]) reveals that the critical currents for switching can be reduced by adopting a perpendicular geometry, in which the layer magnetization is out of the plane. In this situation, in fact, the demagnetizing field is collinear to the anisotropy field. As a consequence, the critical currents for switching are directly proportional to the anisotropy and hence to the stability of the junction. In contrast, in the in-plane geometry the current must overcome an additional contribution, proportional to the saturation magnetization, which does not contribute to the device stability. In junctions with this configuration, known as perpendicular MTJs (pMTJs), a large perpendicular magnetic anisotropy (PMA) is required to overcome the shape anisotropy of the thin film and keep the magnetization out of plane.

State-of-the-art devices are based upon CoFeB/MgO thin films [7], which can reach a TMR of up to 604% at room temperature and 1144% at low temperature [8]. Furthermore, a large PMA has been observed at the CoFeB/MgO interface which is sufficient to achieve a perpendicular geometry in ultrathin layers [9]. Alternatively, $L1_0$ FePt is a popular material choice for high-density magnetic recording since it has a large magnetocrystalline PMA, $K_u = 7 \times 10^6\,\mathrm{Jm}^{-3}$, allowing stable grain sizes down to a few nanometers [10]. Despite the large uniaxial anisotropy, switching has been observed in FePt/Au giant magnetoresistance pillars with the aid of an applied magnetic field [11]. Theoretical calculations of an FePt/MgO MTJ predict a TMR of 340% for an Fe-terminated interface [12].

Unfortunately, growing FePt/MgO devices can be challenging since the lattice mismatch between $L1_0$ FePt and MgO is large, ∼8.5% [13]. This may cause issues during the growth process, such as the inability of preserving the epitaxy across uneven layers. Strain can also cause a significant change in the magnetic properties of the FePt layer. In particular calculations have shown that a strain of 4% can reduce the PMA to about 10% of its original value [11]. Practically, such strain can be reduced by inserting a seed layer with a more amenable lattice constant at the MgO/FePt interface.

In this work we investigate a series of FePt/MgO-based pMTJs in order to establish their potential for future device applications. We utilize *ab initio* models to calculate the spin-transfer torque and the TMR for a range of FePt-based

*sanvitos@tcd.ie

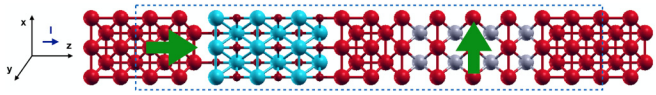

FIG. 1. Setup for a quantum transport calculation of an Fe/MgO/Fe/FePt/Fe junction. The dashed rectangle delimits the scattering region from the leads. The green arrows indicate the different directions of the magnetizations of the magnetic layers on the left- and right-hand sides of the insulating barrier. The colored spheres represent atoms of different species: Fe atoms are in red, Pt atoms are in gray, O atoms are in light blue, Mg atoms are small red spheres.

MTJ structures. We begin by detailing our computational method, before presenting results on the atom-resolved STT in the zero-bias limit for an Fe/MgO/Fe junction. This has an electronic structure analogous to that of CoFeB-based MTJs and hence provides a useful starting point for the discussion. We then continue with the analysis of the torque acting on the MTJs with FePt/Fe free layers and with a thin Fe seed layer intercalated at the MgO interface. In this case we vary the thickness of both the FePt layer and the seed layer (including the case where there is no seed layer). We find that a MgO/FePt interface yields a STT that decays more slowly in the free layer than in the MgO/Fe case, while the insertion of an Fe seed layer produces results similar to the FePt-free case. We then present the outcome of our TMR calculations and the STT acting on the Fe reference layer for some representative cases. Finally, we replace the Fe atoms in the seed layer with Ni. This provides a comparison and helps us to formulate an argument about the origin of the spatial dependence of the STT.

II. COMPUTATIONAL METHOD

Our approach for calculating the spin-transfer torque follows the prescription provided by Haney *et al.* [14] and is based on isolating the transport (nonequilibrium) contribution to the density matrix from the equilibrium part. The influence that an electric current has on the system can be estimated from first principles by combining density functional theory and the nonequilibrium Green's functions method for transport (DFT+NEGF). All calculations have been performed with the SMEAGOL code [15–18], which implements the DFT+NEGF scheme within the numerical atomic orbital framework of the SIESTA package [19].

The system setup for the quantum transport calculation sandwiches the magnetic tunnel junction between two semi-infinite leads (see Fig. 1). These are assumed to be made of bulk material and to be at equilibrium. Note that a certain portion of the electrodes has to be included in the scattering region in order to ensure the continuity of the electrostatic potential. Here the magnetization of the reference or fixed layer $\mathbf{M}_{\rm ref}$ is considered to be magnetized along z (the transport direction), and the one of the free layer $\mathbf{M}_{\rm free}$ is magnetized along x, so that the two form a $\pi/2$ angle. A voltage is applied in such a way that the electron flux is flowing along the stacking direction, z, in our convention from the reference layer to the free one.

The component of the torque vector $\mathbf{T}$ which is responsible for the switching between the parallel and antiparallel magnetization configurations is the one that lies in the plane defined by $\mathbf{M}_{\rm free}$ and $\mathbf{M}_{\rm ref}$, namely, the x-z plane. In the free layer this component coincides with T_z, which is the main focus of our study. In order to reduce the computational costs, we limit our analysis of the torque response to a small bias, the *torkance*, meaning that all calculations are performed in the linear response approximation. At an atom a in the free layer the torkance is defined as

$$\tau_z^a \equiv \frac{dT_z^a}{dV}\Big|_{V=0} = \frac{1}{2}\mathrm{Re}\sum_{i\in a}\sum_j \left(\mathbf{\Delta}_{ij} \times \frac{d\boldsymbol{m}_{ji}}{dV}\Big|_{V=0}\right)_z , \quad (1)$$

and this can be estimated with a zero-bias calculation. Here $\mathbf{\Delta}$ denotes the exchange and correlation field, namely, the derivative of the exchange and correlation energy $E_{\rm XC}$, with respect to the magnetization density $\boldsymbol{m}$, $\mathbf{\Delta} = \delta E_{\rm XC}/\delta \boldsymbol{m}$. Thus, the derivative of $\boldsymbol{m}$ with respect to voltage embodies the spin contribution due to the rearrangement of the electronic population under nonequilibrium conditions. Henceforth, this will be referred to as the nonequilibrium spin density or the spin accumulation. As such, the torque is the result of the interaction between the internal static field $\mathbf{\Delta}$ and the nonequilibrium spin density generated by the current flow. Further details on the calculation of the spin-transfer torque and the torkance can be found in Refs. [20,21].

A series of junctions is constructed, all having a barrier of six MgO layers sandwiched between two semi-infinite leads of bulk bcc Fe oriented along the (001) direction. Periodic boundary conditions are applied in the plane perpendicular to the transport as a result of the perfect epitaxy of the junction. The in-plane lattice constant is taken to be $a_{\rm Fe} = 2.866$Å throughout the system. The out-of-plane lattice constants of the remaining materials were chosen according to information provided in Refs. [13,22], in particular $c_{\rm MgO} = 4.05/\sqrt{2}$ Å, $c_{\rm FePt} = 1.737$Å. The same studies assess that the stablest interfacial configuration is made of an Fe-terminated FePt surface on top of O (Fe) for the FePt/ MgO (FePt/Fe) interface, with an interplane distance of 2.2Å (1.585Å). The accuracy of such estimates was found to be satisfactory by relaxation of the different structures. The local-spin-density approximation (LSDA) for the exchange correlation potential was adopted. A real-space mesh cutoff of 900 Ry along with a 15×15 k-point mesh in the plane orthogonal to transport was found to yield converged results. We adopted double-ζ polarized orbitals for each atomic species, and the convergence of the radial cutoffs was verified by comparing the band structure of bulk materials with the result of all-electron calculations. Finally, all results presented in the next sections were obtained with calculations not including relativistic corrections, unless otherwise stated.

III. RESULTS

We begin by examining the properties of an Fe/MgO/Fe MTJ to later discuss their modification upon the introduction of an FePt layer. As shown in Eq. (1), the torkance is given by the vector product of the exchange and correlation field and the nonequilibrium spin density. Since the free layer is magnetized in the x direction and within the LSDA the exchange and correlation field is proportional and locally parallel to the magnetization, the only relevant components

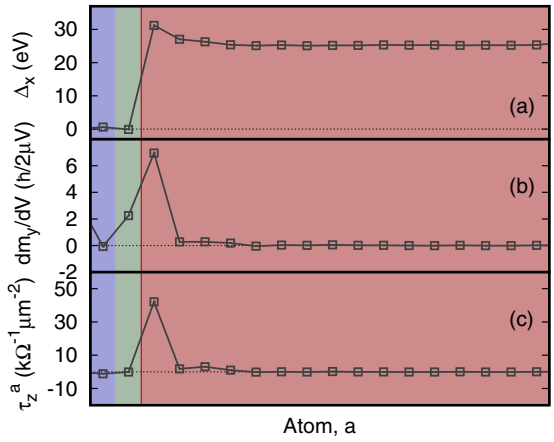

FIG. 2. Real-space profiles of the relevant components of (a) the exchange and correlation field $\mathbf{\Delta}$, (b) the nonequilibrium spin density $d\boldsymbol{m}/dV$, and (c) the torkance $\boldsymbol{\tau}$ per unit μ_B/e and area acting on the bcc Fe free layer. The colored background indicates the atomic species in the stack: red for Fe, blue for O, and green for Mg.

to the torkance are Δ_x and dm_y/dV. These two components and the resulting torkance τ_z are shown in Fig. 2.

In general, Δ_x peaks at the Fe/MgO interface and then presents small oscillations with the period of the interlayer Fe separation a_{Fe}. Such a profile does correlate with the real-space profile of the equilibrium magnetic moment (not displayed), which is also enhanced at the Fe/MgO interface. In contrast, the nonequilibrium spin density [Fig. 2(b)] has an appreciable magnitude only in the region around the Fe/MgO interface. This decays in the Fe layer and is almost fully attenuated a few monolayers from the interface. Such behavior will later be compared with that in FePt and in Ni. Finally, note that there is an appreciable nonequilibrium spin density also in the MgO, although it does not contribute to the torkance since the exchange and correlation field vanishes in the absence of a local magnetization [see Fig. 2(a)].

If we now consider the torkance, we note that this is sharply peaked at the Fe/MgO interface and is attenuated in the Fe layer at the same speed of the nonequilibrium spin density. In fact, for this Fe/MgO/Fe case the spatial dependence of the torkance closely resembles that of the spin accumulation, given the fact that the exchange and correlation field has little spatial dependence on Fe. Let us remark, however, that the point-by-point vector product of the quantities in Figs. 2(a) and 2(b) does not give the torkance in Fig. 2(c) since the sum of the products of the matrix elements does not equal the product of the sums [namely, $\sum_{ij}(\mathbf{\Delta}_{ij}\times\frac{d\boldsymbol{m}_{ji}}{dV})\neq(\sum_i\mathbf{\Delta}_{ii})\times(\sum_i\frac{d\boldsymbol{m}_{ii}}{dV})$; see formula (1)].

We note that the sharpness of the decay obtained in this work differs from the one presented in Ref. [23], where an approach analogous to the one considered here is employed to study the STTs in Cu/Fe/MgO/Fe/Cu junctions. In such work the in-plane component of the torkance in the Fe free layer gradually fades away within five atomic layers from the interface, with a less marked decay than the one shown in Fig. 2. We believe that such a discrepancy is caused by the differences in the system choice and in the simulation parameters. On the one hand, an Fe/Cu free layer, as considered in Ref. [23], may give rise to quantum well states within the Fe film and hence extend the decay range, in contrast to the case of a pure Fe contact. On the other hand, the layer-resolved torkance presented in such work is evaluated at only the Γ point, in contrast to the 15×15 planar k-point grid adopted here. This second aspect is particularly relevant since an adequate sampling of the Brillouin zone is known to be key in order to accurately estimate tunneling properties. This can also be seen by comparing the total torkance in the two cases, as described later in this section.

The remainder of this section is dedicated to a discussion of the modifications introduced by the presence of an FePt stack in the free layer. All results are obtained by neglecting relativistic corrections, with the exception of the data points denoted with blue circles in the left panels of Figs. 3 and 4. From such figures it is evident that the inclusion of spin-orbit interactions (SOIs) does not introduce significant changes in the displayed quantities. This can be understood by comparing the difference in intensity between the SOIs and exchange interactions in the system. The energy associated with spin-orbit interaction in heavy metals such as Pt is typically of the order of tens of meV, in contrast to exchange interaction that is three orders of magnitude stronger [e.g., see Fig. 2(a)]. Moreover, normally, spin-orbit torques drive magnetization dynamics with currents parallel to the interface for lengths of the order of micrometers, in contrast to the nanometer scale considered here. As a consequence, it is reasonable to think that torques originating from spin-obit effects are negligible in this contest.

We now explore the effects of inserting a layer of FePt at the MgO/free layer interface. Figures 3(a)–3(c) show, as with the case of the Fe/MgO/Fe MTJ, the relevant components of $\mathbf{\Delta}$ and $d\boldsymbol{m}/dV$ contributing to the total torkance along z for an FePt layer four unit cells thick. From Fig. 3(a) it is clear that the exchange and correlation field is enhanced at the Fe sites and also finite at the Pt ones. This is because in $L1_0$ FePt there is an induced magnetic moment on the Pt ions (this is about $0.4\mu_B$, as calculated from the Mülliken population analysis), in agreement with previous *ab initio* calculations [13]. The oscillations in the Δ_x profile remain constant in the FePt layer without any sign of decay, and then in the Fe layer the Δ_x profile returns to resembling the one observed before in Fig. 2. Note that $\mathbf{\Delta}$ is an equilibrium property, which essentially depends on the presence of an exchange splitting in a given material. As such, one does not expect a decay of $\mathbf{\Delta}$ unless there is a decay in the magnetization.

In contrast to the pure Fe case, the nonequilibrium spin density has lower intensity in FePt than in Fe but a significantly less attenuated decay [Fig. 3(b)]. The total nonequilibrium spin density shows regular oscillations within the FePt layer, while it is enhanced at both the FePt/Fe and MgO/FePt interfaces, and then vanishes within a few unit cells of the Fe lead. Furthermore, we observe that dm_y/dV in Pt has the opposite sign with respect to that of the first Fe layer in contact with MgO. Finally, the torkance [Fig. 3(c)] is again peaked at the interface with MgO, but its strength is reduced in comparison to that computed for the Fe/MgO/Fe MTJ with the same MgO thickness. Within the FePt layer the torkance does not attenuate as in Fe but persists to reach the Fe-only side of the free layer. Most interestingly, the torkance has an

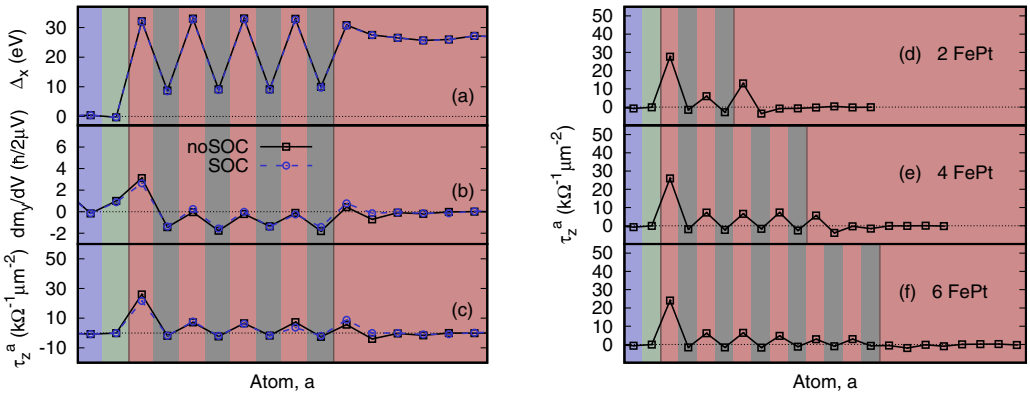

FIG. 3. Study of the torkance in an FePt/Fe free layer. Left: the relevant components of (a) the exchange and correlation field $\mathbf{\Delta}$, (b) the nonequilibrium spin density $d\boldsymbol{m}/dV$, and (c) the torkance per unit of μ_B/e and area $\boldsymbol{\tau}$. Black squares and blue circles indicate results obtained without and with relativistic corrections, respectively. Right: comparison of the torkance per unit μ_B/e and area of MTJs with (d) two, (e) four, and (f) six FePt unit cells. In both columns the colored background indicates the atomic species: red for Fe, gray for Pt, blue for O, and green for Mg.

oscillatory behavior in FePt, presenting small negative values at the Pt layers and positive values at the Fe ones. Such oscillations are common in antiferromagnets [20] and here are observed also in a ferromagnet with nontrivial magnetic texture. It is also interesting to note that, despite the larger spin accumulation at Pt sites, the resulting torque is smaller than that at the Fe ones. This is due to the fact that the exchange and correlation field in Pt is significantly weaker than in Fe (because the magnetization is smaller).

The persistence of the torkance in the FePt layer remains as we change the FePt thickness n_{FePt} (number of unit cells). This can be seen in the Figs. 3(d)–3(f). For a thin layer [Fig. 3(d)] the torque is enhanced at the FePt/Fe interface, while it is attenuated for all the other cases [e.g., see $n_{\mathrm{FePt}} = 6$ in Fig. 3(f)]. Furthermore, for all the thicknesses considered, the torkance remains strikingly positive at all the Fe atomic planes of FePt, while it is small and negative at the Pt ones. Moreover, the intensity of the peak at the MgO/FePt is not modified by the increase in thickness.

Although Fe/MgO/FePt/Fe junctions provide an interesting case of study, the significant lattice mismatch between MgO and $L1_0$ FePt (∼8.5%) makes their experimental realization troublesome. This problem may be overcome by inserting a compatible seed layer at the MgO/FePt interface. Hence, we have analyzed the influence of incorporating a thin Fe seed layer (SL) between the MgO and the FePt, keeping the thickness of the FePt layer constant at four unit cells. The Fe SL has different effects depending on its thickness (see Fig. 4). We notice from Fig. 4(a) that the exchange and correlation field profile in FePt is analogous to the previous case (since the equilibrium magnetization profile is also unchanged), while Δ_x is almost constant in the seed layer. The nonequilibrium spin density still oscillates in FePt, although the amplitude of such oscillations is much smaller than that obtained in the absence of the SL. Consequently, the torkance [Fig. 4(c)] is peaked at the MgO/Fe interface with the SL, and its intensity is comparable to that observed for the Fe/MgO/Fe case (see Fig. 3). The torkance, however, is not exactly zero away from

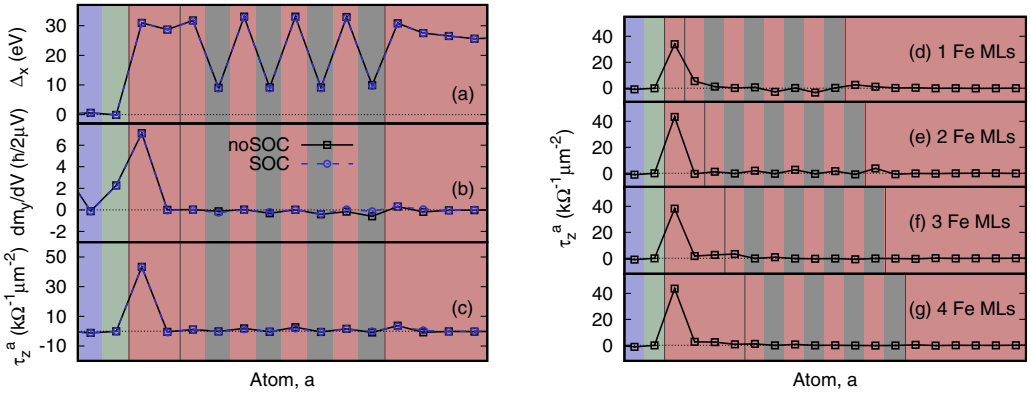

FIG. 4. Study of the torkance in an Fe/FePt/Fe free layer made of four FePt monolayers and a variable number of Fe monolayers inserted between MgO and FePt. Left: the relevant components of (a) the exchange and correlation field $\mathbf{\Delta}$, (b) the nonequilibrium spin density $d\boldsymbol{m}/dV$, and (c) the torkance per unit of μ_B/e and area $\boldsymbol{\tau}$. Black squares and blue circles indicate results obtained without and with relativistic corrections, respectively. Right: comparison of the torkance per unit μ_B/e and area of MTJs with a seed layer comprising (d) one, (e) two, (f) three, and (g) four Fe monolayers. In all panels the colored background indicates the atomic species: red for Fe, gray for Pt, blue for O, and green for Mg.

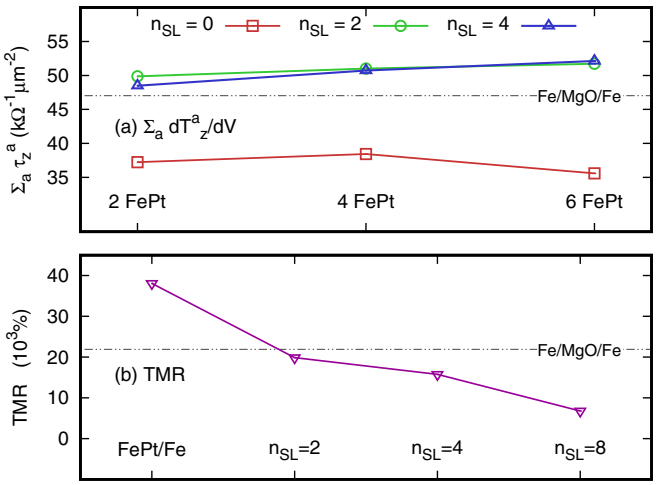

FIG. 5. (a) The total torkance per unit μ_B/e and area acting on the free layer of Fe/MgO/Fe/FePt/Fe junctions with two, four, and six FePt monolayers and an Fe seed layer of $n_{SL} = 0, 2, 4$ atomic planes. (b) The calculated TMR in Fe/MgO/FePt(4)/Fe and Fe/MgO/Fe(n_{SL})/FePt(4)/Fe junctions where the number in the parentheses indicates the number of unit cells in each layer with $n_{SL} = 2, 4, 8$ Fe unit cells. In both graphs the black dashed line represents the same quantity calculated for the Fe/MgO/Fe junction.

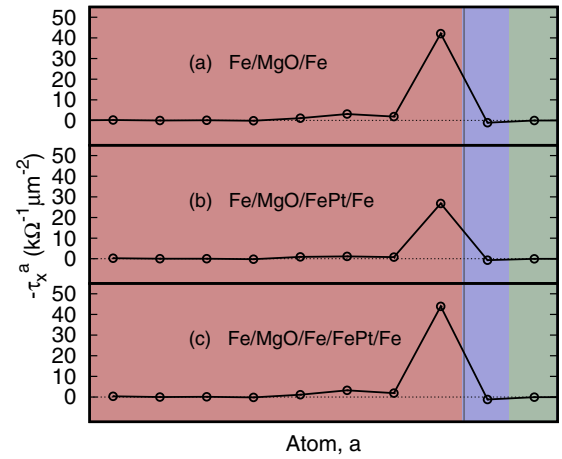

FIG. 6. Torkance per unit μ_B/e and area acting on the reference layer of (a) Fe/MgO/Fe, (b) Fe/MgO/FePt(4)/Fe, and (c) Fe/MgO/Fe(2)/FePt(4)/Fe MTJs. The colored background indicates the atomic species to which each point corresponds: red for Fe, blue for O, and green for Mg.

the SL, in particular on the Fe atoms of FePt and at the FePt/Fe interface. This does not happen for thicker Fe SLs [Figs. 4(f) and 4(g)], for which the total torkance decays before reaching the interface with FePt. We note that in cases where the SL is composed of an odd number of layers [Figs. 4(d) and 4(f)] the decay of the torkance is slightly less pronounced in the seed layer. In general, however, the main effect of the seed layer is to suppress the persistence of the torkance in FePt, so that all the angular momentum transfer takes place in the seed layer.

We now move to analyzing the total torkance and the TMR of each junction. Figure 5(a) shows the total torkance integrated over the free layer, $\tau_z^{\rm tot} = \sum_a^{\alpha\in {\rm FL}} \tau_z^a$, for different thicknesses of the FePt layer. We present results for the situation where there is no SL (red squares) and for an Fe SL of 2 (green circles) and 4 (blue triangles) atomic planes, while the black line shows the value obtained for the Fe/MgO/Fe case. For each SL thickness, the torkance shows little dependence on the thickness of the FePt layer. When there is no SL, this is attributed to the oscillatory behavior without attenuation of the torkance profile as observed in Fig. 3. In contrast, when a SL is present, most of the torque resides at the first MgO/Fe interface, so that the thickness of the FePt becomes irrelevant (see Fig. 4). Interestingly, when a SL is present, the total torkance transferred into the Fe/MgO/Fe/FePt MTJ is larger than that of a simpler Fe/MgO/Fe MTJ with an identical barrier (dashed black line). This is no longer true when the SL is absent. Such a finding means that the introduction of an Fe seed layer not only helps in achieving a better epitaxy during the growth but also facilitates a larger spin-transfer torque. More generally, we can conclude that any modification introduced in the free layer outside the decay range of the torque has little to no consequence on the total torque. This is also in agreement with the findings presented in Ref. [23], although the total torkance for a pure Fe free layer displayed in that work is about 75% of the one shown in Fig. 5(a). Nevertheless, the former considers contributions due to only the Γ point, which is the most likely cause of such a discrepancy.

Figure 5(b) shows the calculated TMR for each junction (in all cases the FePt layer comprises four layers) and a comparison with that of an Fe/MgO/Fe MTJ with an identical barrier. We observe that the junction with no Fe SL presents the largest TMR, despite having the lowest torkance. This is unexpected since in FePt bands with Δ_1 symmetry, namely, those with the largest transmission across MgO, are present for both spin channels [12]. Such a feature returns a predicted TMR for MTJs with FePt leads not exceeding 340% [12]. However, here the situation is different since in all our MTJs the leads are made of Fe, so that spin filtering is always in place. As such, in our case the addition of an FePt layer (or a complex Fe/FePt layer) changes the details of the spin-dependent scattering potential but does not alter the main spin-filtering mechanism at play in Fe/MgO/Fe junctions. Interestingly, as the thickness of the Fe SL gets larger, the value of the TMR is reduced.

So far the left electrode has been considered to be the fixed layer, namely, the one producing the spin-polarized current. It is now interesting to look at the opposite case, namely, the one where the electron flux flows from the right-hand to the left-hand electrode. This is the situation where the FePt/Fe composite electrode acts as the fixed, current-polarizing layer. Since in the right electrode the magnetization is along the z direction, the relevant torque in this case is τ_x. This is presented in Figs. 6(a)–6(c) for three representative junctions: Fe/MgO/Fe, Fe/MgO/FePt(4)/Fe, and Fe/MgO/Fe(2)/FePt(4)/Fe, respectively, where the numbers in parentheses indicate the number of unit cells. Since in this geometry the current flows in the direction opposite that in the previous case, we have plotted $-\tau_x$, namely, the torque component that will lead to an alignment of the magnetizations of the fixed and free layers. The trend of $-\tau_x$ is in all cases analogous to that of τ_z for the Fe/MgO/Fe MTJ [see Fig. 2(c)]; namely, the STT is peaked at the magnet/insulator interface

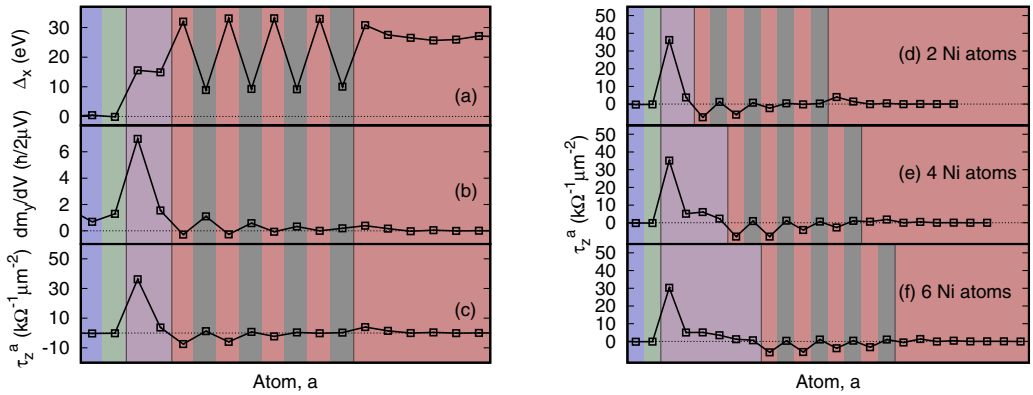

FIG. 7. Study of the torkance in an Fe/MgO/Ni/FePt/Fe junction with different Ni seed layer thicknesses. Left: the relevant components of (a) the exchange and correlation field $\mathbf{\Delta}$, (b) the nonequilibrium spin density $d\boldsymbol{m}/dV$, and (c) the torkance per unit of μ_B/e and area $\boldsymbol{\tau}$. Right: comparison of the torkance per unit μ_B/e and area of MTJs with a seed layer comprising (d) two, (e) four, and (f) six Ni monolayers. The colored background represents the different atomic species: red for Fe, gray for Pt, blue for O, green for Mg, and purple for Ni.

and is negligible elsewhere. The only significant difference between the three MTJs is the reduction of approximately a factor of 2 of the peak intensity for the Fe/MgO/FePt(4)/Fe stack [Fig. 6(b)].

IV. DISCUSSION

The results presented so far indicate that the STT (the torkance) varies strongly with the distance from the MgO interface and that the details depend subtly on the specific layer structure. In general, Fe seems capable of absorbing a significant amount of angular momentum, so that only a few Fe monolayers are enough to make the STT decay sharply from the MgO interface. The main cause of such an effect has to be found in the intense Fe exchange field. In fact, the strong exchange interaction in Fe relaxes the nonequilibrium spin density (the spin accumulation) toward the local direction of the magnetization within a few atomic layers of the interface, so that there is little $d\boldsymbol{m}/dV$ away from the interface itself. In addition the exchange and correlation field remains almost constant within the Fe layer, resulting in a torque that persists little away from the interface with MgO.

In $L1_0$ FePt the alternating planes of Fe and Pt lead to a magnetization texture that is nonuniform at the atomic scale. In particular $\mathbf{\Delta}$ is small at the Pt sites, so that the average exchange and correlation field is reduced with respect to that of the pure Fe case. As a consequence, the spin accumulation can penetrate longer into the free layer so that the STT decays less sharply. In order to further investigate the effects of the exchange field on the spatial decay of the torque we now consider a Ni seed layer since it has a much smaller moment, and thus exchange field, than Fe. The calculation has been simplified by maintaining the bcc structure and the lattice constant of Fe. As such our device stack does not correspond to a likely experimental situation but just serves the purpose of comparing the different seed layers. The atomic-resolved torkance for a Fe/MgO/Ni/FePt/Fe stack with a Ni seed layer comprising two, four, and six atomic planes is shown in Fig. 7.

As in the case of an Fe seed layer, the torque [Fig. 7(c)] is strongly peaked at the Ni/MgO interface, but now it does not decay entirely, and thus, a nonvanishing STT with an oscillatory behavior persists into the FePt layer. A closer look at the profile of $\mathbf{\Delta}$ across the junction [Fig. 7(a)] reveals that the exchange and correlation field in Ni is about half of that of Fe [see Fig. 4(a)]. As a consequence, in Ni the spin accumulation does not relax along the local direction of the magnetization as efficiently as in Fe, a fact that can be appreciated by comparing Fig. 7(b) with Fig. 4(b). Interestingly, the attenuation of the spin accumulation and thus of the torque is not complete even for relatively thick Ni seed layers, as can be seen in Figs. 7(d) through 7(f). A second interesting observation concerns the phase of the oscillations of the STT in the FePt layer. In fact for a junction where FePt is in direct contact with the MgO barrier, the torque is positive at the Fe planes and negative (although rather small) at the Pt ones. The same behavior, although with a much reduced torque is observed for Fe intercalation (in the presence of an Fe seed layer). In contrast when the seed layer is made of Ni the sign of the STT on the FePt layer changes, becoming negative at the Fe planes and positive (although small) at the Pt ones. As a result the total integrated torque over the entire free layer (seed layer plus FePt) for Ni intercalation is two thirds of that obtained with Fe intercalation.

Finally, we wish to make a few general remarks on the spatial dependence of the STT. Macroscopic models combining the Landau-Lifshitz-Gilbert equation for the magnetization dynamics with a diffusion model for the spin accumulation [24,25] suggest that the spin accumulation is maximized in regions where there is a large magnetization gradient, namely, at interfaces. This is confirmed here at the microscopic level. In all cases investigated we find the maximum spin accumulation, and hence torque, at the interface between the free layer and MgO regardless of the presence of a seed layer. Furthermore, we also find an enhanced spin accumulation and torque at the second interface between the free layer and the Fe lead, although this is small since the spin accumulation always decays in the free layer. The fine details of the spin accumulation profile depend on how the entire stack responds to the application of an external bias. This in turn is affected by the reorganization in the occupation of

the states around the Fermi surface, which is indeed a subtle effect.

In general a large exchange splitting causes the spin accumulation to relax faster along the local magnetization direction. As such, we expect the spin accumulation to decay more severely in the free layer of stacks where there is a large torque at the first few atomic layers in contact with the MgO barrier. This in turn depends on the strength of the exchange and correlation field, which in the LSDA can be written as

$$\mathbf{\Delta}^{\mathrm{LSDA}}(\mathbf{r}) = \frac{\delta E_{\mathrm{XC}}^{\mathrm{LSDA}}}{\delta \mu_{\mathrm{B}} \mathbf{m}(\mathbf{r})} = -\frac{\partial \epsilon_{\mathrm{XC}}}{\partial m(\mathbf{r})} \frac{n(\mathbf{r})}{\mu_{\mathrm{B}}} \frac{\mathbf{m}(\mathbf{r})}{m(\mathbf{r})}, \quad (2)$$

where $\mathbf{m}(\mathbf{r})$ is the local magnetization vector, $m(\mathbf{r}) = |\mathbf{m}(\mathbf{r})|$, $E_{\mathrm{XC}}^{\mathrm{LSDA}}$ is the LSDA exchange and correlation energy, ϵ_{XC} is the exchange and correlation energy density of the homogeneous electron gas, $n(\mathbf{r})$ is the charge density, and μ_{B} is the Bohr magneton. Crucially, the LSDA $\mathbf{\Delta}$ is locally parallel to the magnetization direction. As such, one expects $\mathbf{\Delta}$ (and hence the torque) to change sign as the local magnetization changes sign (as in the case of antiferromagnets). Furthermore, one can show that $|\mathbf{\Delta}| \sim Im$, where I is the Stoner parameter [26]. This means that for similar Stoner coupling the exchange and correlation field is more intense for materials presenting larger magnetization. This last feature explains the difference in $\mathbf{\Delta}$ and torque between the Fe and the Ni seed layer. In fact Fe and Ni have rather similar Stoner parameters, but their magnetizations differ by more than a factor of 3.

V. CONCLUSIONS

In conclusion, we have calculated the STT acting upon the free ferromagnetic layer in a series of FePt-based magnetic tunnel junctions. For a simple Fe/MgO/Fe MTJ the torkance is peaked at the MgO interface and decays within four atomic planes. When the stack is modified to include FePt (Fe/MgO/FePt/Fe) the torkance decays much slower and persists into the free layer up to at least 12 atomic planes. Such retention is associated with torkance oscillations at the length scale of the Fe-Pt plane separation. Since the lattice mismatch between MgO and FePt is large, we have explored the option to intercalate an Fe seed layer at the interface between MgO and FePt. Also in this case the torkance is significant only at the first MgO/Fe interface, and it vanishes in FePt. This is the result of the strong reduction of the spin accumulation beyond the Fe seed layer. Such strong attenuation appears to originate from the large exchange and correlation field in Fe, which rapidly aligns the spin accumulation along the local direction of magnetization. Such a hypothesis is confirmed by calculations for the STT in some hypothetical MTJs incorporating a Ni seed layer. Since Ni has an exchange and correlation field that is weaker than that of Fe, it is less effective at suppressing the spin accumulation (in absorbing angular momentum), and thus, the attenuation of the torkance is weaker. Altogether our results suggest that the atomic and material details of the MTJ stack play an important role in determining the total STT that a free layer can experience. This knowledge can help in designing stacks with maximal torkance, so that a reduction in the critical current for switching can be achieved.

ACKNOWLEDGMENTS

This work has been supported by the Science Foundation Ireland Principal Investigator award (Grants No. 14/IA/2624 and No. 16/US-C2C/3287) and TCHPC (Research IT, Trinity College Dublin). The authors wish to acknowledge the DJEI/DES/SFI/HEA Irish Centre for High-End Computing (ICHEC) for the provision of computational facilities and support.

[1] J.-G. Zhu and C. D. Park, Mater. Today **9**, 36 (2006).
[2] S. Parkin, Xin Jiang, C. Kaiser, A. Panchula, K. Roche, and M. Samant, Proc. IEEE **91**, 661 (2003).
[3] M. Julliere, Phys. Lett. A **54**, 225 (1975).
[4] J. Slonczewski, J. Magn. Magn. Mater. **159**, L1 (1996).
[5] D. C. Ralph and M. D. Stiles, J. Magn. Magn. Mater. **320**, 1190 (2008).
[6] S. Mangin, D. Ravelosona, J. A. Katine, M. J. Carey, B. D. Terris, and E. E. Fullerton, Nat. Mater. **5**, 210 (2006).
[7] J. M. Slaughter, Annu. Rev. Mater. Res. **39**, 277 (2009).
[8] S. Ikeda, K. Miura, H. Yamamoto, K. Mizunuma, H. D. Gan, M. Endo, S. Kanai, J. Hayakawa, F. Matsukura, and H. Ohno, Nat. Mater. **9**, 721 (2010).
[9] D. C. Worledge, G. Hu, D. W. Abraham, J. Z. Sun, P. L. Trouilloud, J. Nowak, S. Brown, M. C. Gaidis, E. J. O'Sullivan, and R. P. Robertazzi, Appl. Phys. Lett. **98**, 022501 (2011).
[10] D. Weller, A. Moser, L. Folks, and M. Best, IEEE Trans. Magn. **36**, 10 (2000).
[11] T. Seki, S. Mitani, K. Yakushiji, and K. Takanashi, Appl. Phys. Lett. **88**, 172504 (2006).
[12] Y. Taniguchi, Y. Miura, K. Abe, and M. Shirai, IEEE Trans. Magn. **44**, 2585 (2008).
[13] R. Cuadrado and R. W. Chantrell, Phys. Rev. B **89**, 094407 (2014).
[14] P. M. Haney, D. Waldron, R. A. Duine, A. S. Núñez, H. Guo, and A. H. MacDonald, Phys. Rev. B **76**, 024404 (2007).
[15] A. R. Rocha, V. M. García-Suárez, S. W. Bailey, C. J. Lambert, J. Ferrer, and S. Sanvito, Nat. Mater. **4**, 335 (2005).
[16] A. R. Rocha, V. M. García-Suárez, S. W. Bailey, C. J. Lambert, J. Ferrer, and S. Sanvito, Phys. Rev. B **73**, 085414 (2006).
[17] I. Rungger and S. Sanvito, Phys. Rev. B **78**, 035407 (2008).
[18] I. Rungger, O. Mryasov, and S. Sanvito, Phys. Rev. B **79**, 094414 (2009).
[19] J. M. Soler, E. Artacho, J. D. Gale, A. García, J. Junquera, P. Ordejòn, and D. Sànchez-Portal, J. Phys.: Condens. Matter **14**, 2745 (2002).
[20] M. Stamenova, R. Mohebbi, J. Seyed-Yazdi, I. Rungger, and S. Sanvito, Phys. Rev. B **95**, 060403 (2017).

[21] M. O. A. Ellis, M. Stamenova, and S. Sanvito, Phys. Rev. B **96**, 224410 (2017).

[22] A. Kohn, N. Tal, A. Elkayam, A. Kovacs, D. Li, S. Wang, S. Ghannadzadeh, T. Hesjedal, and R. C. C. Ward, Appl. Phys. Lett. **102**, 062403 (2013).

[23] C. Heiliger and M. D. Stiles, Phys. Rev. Lett. **100**, 186805 (2008).

[24] C. Abert, M. Ruggeri, F. Bruckner, C. Vogler, G. Hrkac, D. Praetorius, and D. Suess, Sci. Rep. **5**, 14855 (2015).

[25] C. J. García-Cervera and X.-P. Wang, J. Comput. Phys. **224**, 699 (2006).

[26] J. Simoni, M. Stamenova, and S. Sanvito, Phys. Rev. B **96**, 054411 (2017).